Journal of the European Ceramic Society 22 (2002) 1389–1394

www.elsevier.com/locate/jeurceramsoc

Crystallographic and microchemical characterization of the early stages of eutectoid decomposition in MgO-partially stabilized ZrO_2

Tomasz Czeppe, Paweł Zięba*, Andrzej Pawłowski

Institute of Metallurgy and Materials Science, Polish Academy of Sciences, Reymonta St. 25, 30-059 Cracow, Poland

Received 16 November 2000; received in revised form 31 January 2001; accepted 16 February 2001

Abstract

The early stages of eutectoid decomposition in ZrO_2-8 mol% and 11 mol% MgO were studied by means of analytical electron microscopy. The observed reaction products at the grain boundaries were monoclinic or tetragonal ZrO_2 phases and MgO precipitates of two different "cellular" morphologies. The application of energy dispersive X-ray microanalysis led to the detection of an abrupt change in the MgO content in the m-ZrO_2 phase, indicating that the eutectoid decomposition in ZrO_2–MgO is controlled by interface rather than volume diffusion. The crystallographic relationships between the parent phase and decomposition products were also determined.

Keywords: Electron microscopy; Eutectoid decomposition; Grain boundaries; MgO; ZrO_2

1. Introduction

The ZrO_2–MgO solid solution (SS) is a key component of partially stabilized (PSZ) ceramic in which small ellipsoidal-shaped precipitates of a tetragonal (t) phase appear in a cubic (c) matrix after appropriate sintering. Subsequent isothermal annealing in the temperature range 1100–1300 °C involves the eutectoid decomposition of the cubic (c-ZrO_2) solute-rich matrix phase into MgO and a solute-depleted tetragonal (t-ZrO_2) or monoclinic (m-ZrO_2) phase according to the following scheme:

$$(\text{c-}ZrO_2\text{SS}) \xrightarrow{>1240^\circ\text{C}} MgO + (\text{t} - ZrO_2)$$

$$(\text{c-}ZrO_2\text{SS}) \xrightarrow{<1240^\circ\text{C}} MgO + (\text{m} - ZrO_2)$$

The eutectoid decomposition in Mg-PSZ was studied by Hannik et al.[1] and Farmer et al.[2,3] The phase constitution after the decomposition was dependent on the thermal history of the material. The reaction started at the original grain boundaries and then the coupled growth of the MgO and solute-depleted m-ZrO_2 SS into c-ZrO_2 SS with t-ZrO_2 precipitates was observed. The morphology of MgO was rod-like with a well-defined orientation relationship to m-ZrO_2.[3] The m-ZrO_2 phase grew in different crystallographic variants. Similar observations were carried out for 8.1 and 11.3 mol% Mg-PSZ.

The present study was undertaken in order to determine the crystallographic and microchemical features of the early stages of the eutectoid reaction in the ZrO_2-8 mol% and 11 mol% MgO. The technique of analytical electron microscopy (AEM) was used, *for the first time*, in order to determine the local changes of the solute content which accompany the formation of eutectoid products.

2. Experimental

Partially stabilized ZrO_2 alloys containing 8.0 and 11.0 mol% MgO (nominal composition) were prepared from a starting ZrO_2 powder of 99.5% purity and 1 μm grain size. Sintering to ≈95% of theoretical density was carried out at 1750 °C for 3 h. Then the samples (pills 8 mm in diameter and 1 mm thick) were slowly cooled within the furnace to room temperature. According to the equilibrium phase diagram of the ZrO_2–MgO system,[2]

* Corresponding author.
E-mail address: nmzieba@imim-pan.krakow.pl (P. Zieba).

0955-2219/02/$ - see front matter
PII: S0955-2219(02)00033-X

the ZrO_2-8.0 and 11 mol% MgO alloys consisted of c-phase at the sintering temperature of 2025 K. Afterwards slow cooling to room temperature ensured the transition through the ((c + t)-ZrO_2), (t-ZrO_2) + MgO and the (m-ZrO_2) + MgO phase compositions.

The applied procedure resulted in an average grain size of 10–20 μm in the samples and partial decomposition due to the eutectoid reaction. The volume fraction of eutectoid reaction products did not exceed 10–20%, as was estimated using transmission electron microscopy (TEM). The MgO concentration in the specimens analyzed by electron probe microanalysis varied by about 10% relative from the nominal composition between particular grains.

In order to produce thin foils for TEM studies, the samples were mechanically thinned down to the thickness 0.1 μm. Then discs 3 mm in diameter were cut off from the slices and ion beam thinned in a GATAN Duomill instrument at 6 kV, until perforation occurred. The final operation was coating of the thin foil with carbon in order to prevent any influence of electrical charging during sample examination.

Energy dispersive X-ray (EDX) analysis was carried out with a Philips CM 20 transmission electron microscope twin operating at 200 kV in the nanoprobe mode with a LaB_6 filament. The analysis was carried out with the orientation of the grain boundary parallel to the incident electron beam, and stepping the probe manually across the region of interest which ensured that the adjacent investigated volumes were spatially resolved. When any visible drift of the specimen was observed, the position of the probe was corrected. A nominal probe diameter of 5 nm, at the "full width at half maximum" was used. The specimen thickness in the region of interest was determined using a contamination spot method and was commonly found to be about 200 nm.

The EDX analysis was performed with the use of an EDAX Phoenix energy dispersive spectrometer, for a

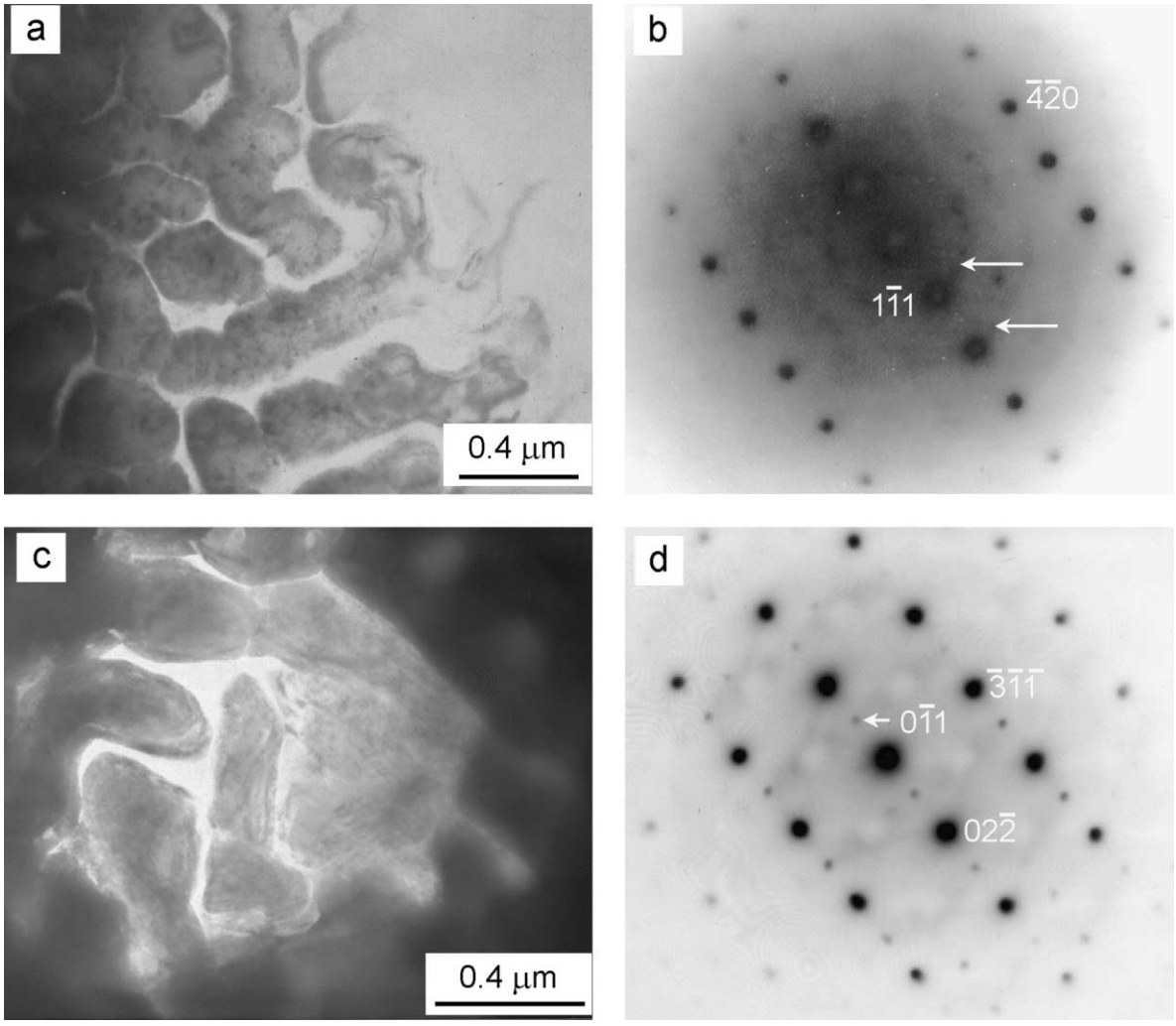

Fig. 1. Eutectoid decomposition in ZrO_2 stabilized with 8 mol% MgO (a, b), and 11 mol% MgO (c, d). Bright-field electron micrographs (a and c). Selected area diffraction patterns taken at: (b) [$\bar{1}$23] zone axis of c-ZrO_2, note the ring-type diffraction from fine-crystalline phase, (d) [$\bar{2}\bar{3}$3] zone axis of t-ZrO_2.

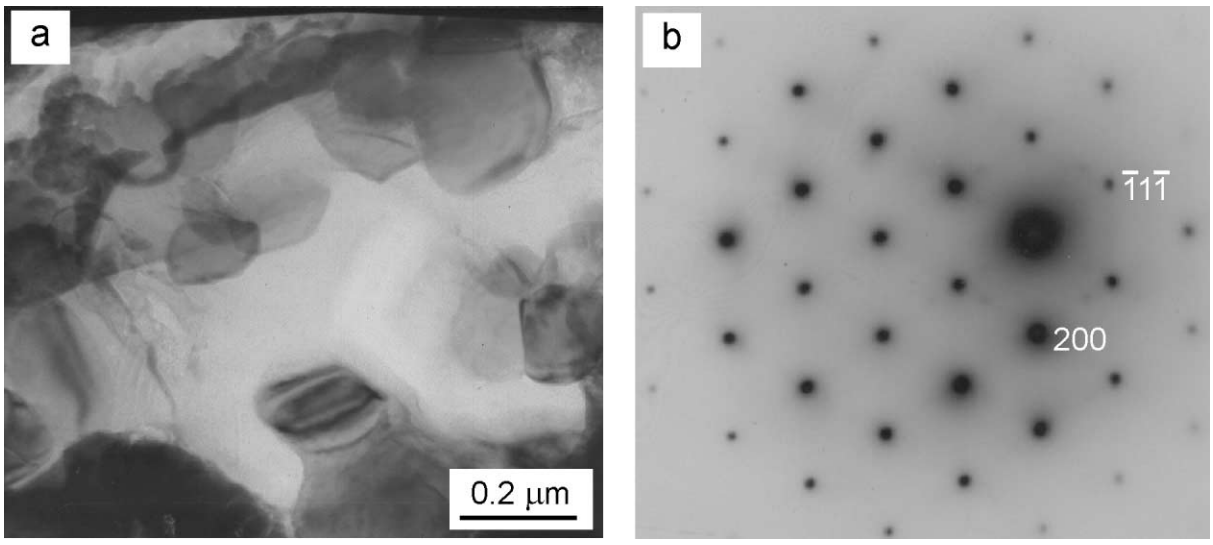

Fig. 2. Precipitates of MgO in ZrO_2 stabilized with 8 mol% MgO. Bright-field electron micrograph (a) and selected area diffraction pattern taken at zone axis [011] of MgO (b).

time sufficient to acquire a few thousand X-ray counts of the analysed elements. The atomic percentage of MgO and ZrO_2 was normalized by the "oxide" formula and virtual standards being an integral part of the Phoenix software. The resulting relative accuracy of the analysis was between 10 and 15%.

3. Results and discussion

Two different morphologies of the eutectoid decomposition were identified. The first one is shown in Fig. 1 while the second one is in Figs. 3 and 4. The first morphology consists of rounded precipitates which are visible in the c-ZrO_2 SS (Fig. 1a and c). The phase microstructure looks similar but selected area diffraction pattern (SADP) revealed some difference. For the sample containing 8 mol% MgO, SADP suggests the cubic ZrO_2 structure (Fig. 1b). For the sample containing 11 mol% MgO the additional diffraction spots (marked by an arrow) from the tetragonal structure were visible (Fig. 1d). In both examples, the "bright" phase visible in the micrographs was partially amorphous, partially fine-crystalline, giving the diffraction pattern in the form of the rings of intensity (marked by arrows in Fig. 1b) in which also precise diffraction spots exist. The chemical composition of this phase was found to be nearly the same as in the matrix of 8 mol% MgO containing the sample and enriched in MgO in the 11 mol% MgO sample. When MgO was observed in the form of regular-shape precipitates, it revealed a typical monocrystalline structure (Fig. 2).

The development of the second type of morphology occurs in two steps. Fig. 3 shows an original grain boundary (GB) of the material occupied by two single precipitates of the phase rich in MgO. A closer inspection using the EDX analysis revealed the concentration close to pure MgO. A characteristic GB bowing between the precipitates clearly indicates that the GB has already moved by the distance of about 400–500 nm. The region swept by the GB is MgO-depleted with an abrupt change in MgO content at the moving interface. This confirms that the boundary acts as a diffusion path feeding the precipitates in solute atoms. The observed behaviour shows similarity with de-alloying during diffusion-induced grain boundary migration preceding the formation of discontinuous precipitates in metallic alloys.[4] The next step is associated with the formation of a cellular structure as is shown in Fig. 4a, where the rod-like MgO precipitates are not connected with the former GB precipitates. This is typical for metallic alloys but in our case they nucleate directly at

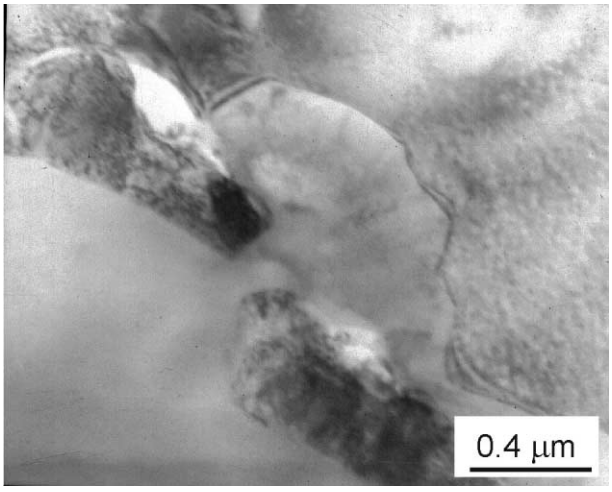

Fig. 3. Bright-field electron micrograph showing the early stage grain boundary migration between two pinning MgO precipitates in ZrO_2 stabilized with 11 mol% MgO.

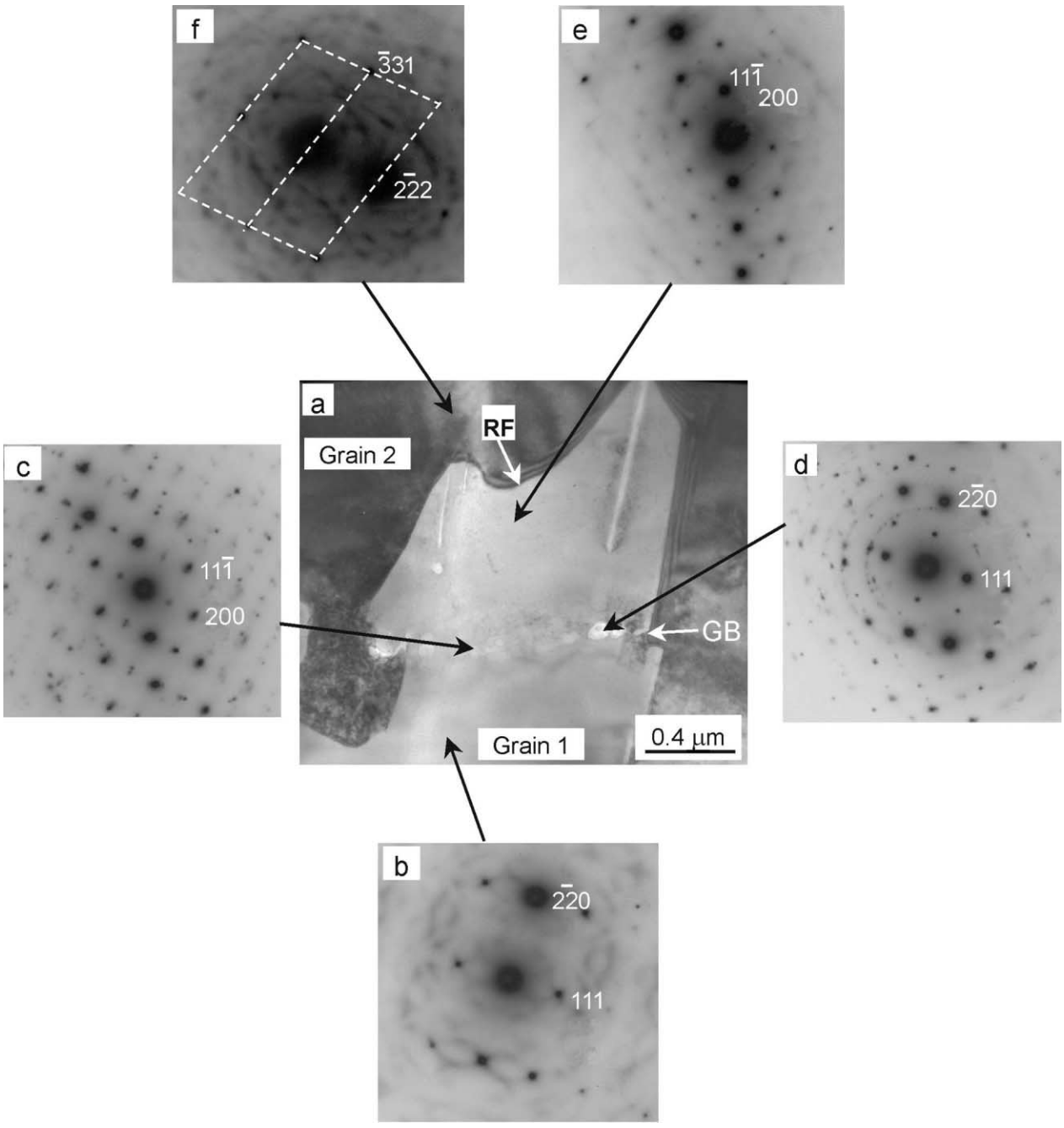

Fig. 4. Bright-field electron micrograph showing grain boundary zone decomposed by the grain boundary diffusion in ZrO_2 stabilized with 8 mol% MgO. (a) Selected area diffraction patterns taken from different areas marked by arrows: (b) zone axis $[11\bar{2}]$ of c-ZrO_2, (c) zone axis [011] of m-ZrO_2, (d) zone axis $[11\bar{2}]$ of m-ZrO_2, (e) zone axis [011] of m-ZrO_2 and (f) zone axis $[1\bar{2}\bar{3}]$ of c-ZrO_2. GB, original grain boundary; RF, reaction front.

the moving interface due to the local solute accumulation. This is somewhat similar to the Fournelle–Clark[5] mechanism of discontinuous precipitation. The substantial difference, however, is that in the Fournelle–Clark model, the movement of the GB occurs without the presence of any precursor precipitates at the GB. The shape of the moving interface is convex, which suggests that the diffusion process is not fast enough to relax the ''pinning'' forces acting on the migrating boundary. As a consequence, the velocity of the GB movement can also be reduced.

The SADP analysis showed the same crystallographic orientation at the original location of the grain boundary and in the zone transformed by the moving reaction front of the eutectoid decomposition (Fig. 4c and e), both occupied by the m-ZrO_2 phase. In Fig. 4d 'rings' of diffraction spots from fine-crystalline MgO precipitate are also visible. The same crystallographic orientation

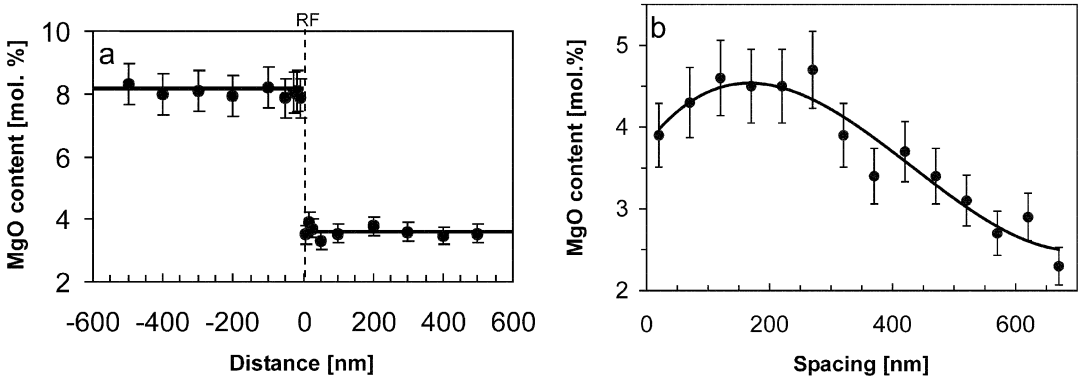

Fig. 5. MgO concentration profiles performed across the reaction front (RF) (a) and across the transformed zone (b) in Fig. 4a.

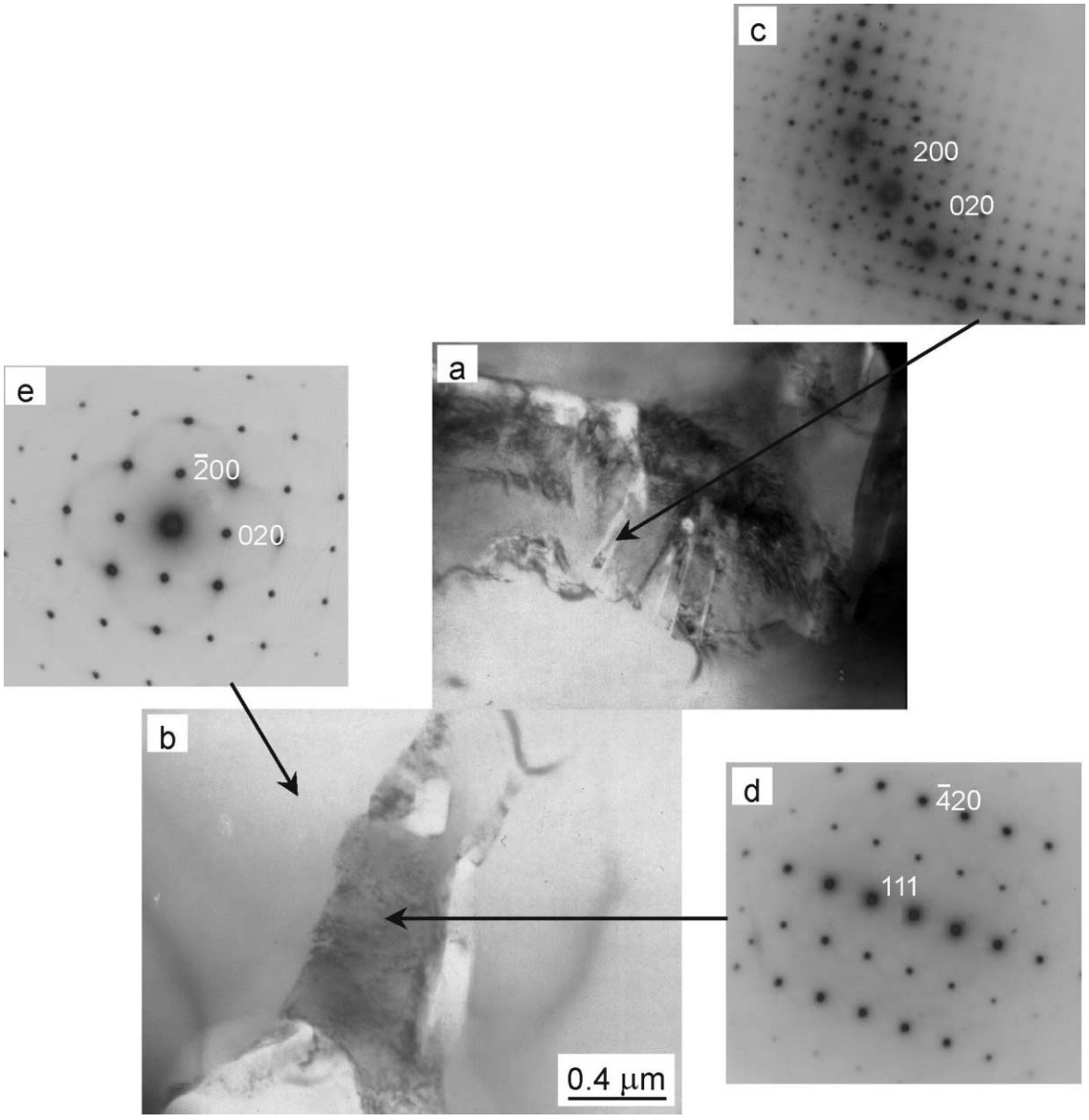

Fig. 6. Bright field electron micrographs of the transformed area at the grain boundaries of ZrO_2 stabilized with 11 mol% MgO showing (a) monoclinic phase of ZrO_2 together with MgO rods; and (b) tetragonal ZrO_2 phase with MgO precipitates and cubic ZrO_2 surrounding grains. The selected area diffraction patterns taken at: (c) zone axis $[00\bar{1}]$ of m-ZrO_2, (d) zone axis $[1\bar{2}\,\bar{3}]$ of t-ZrO_2 and (e) zone axis [001] of c-ZrO_2.

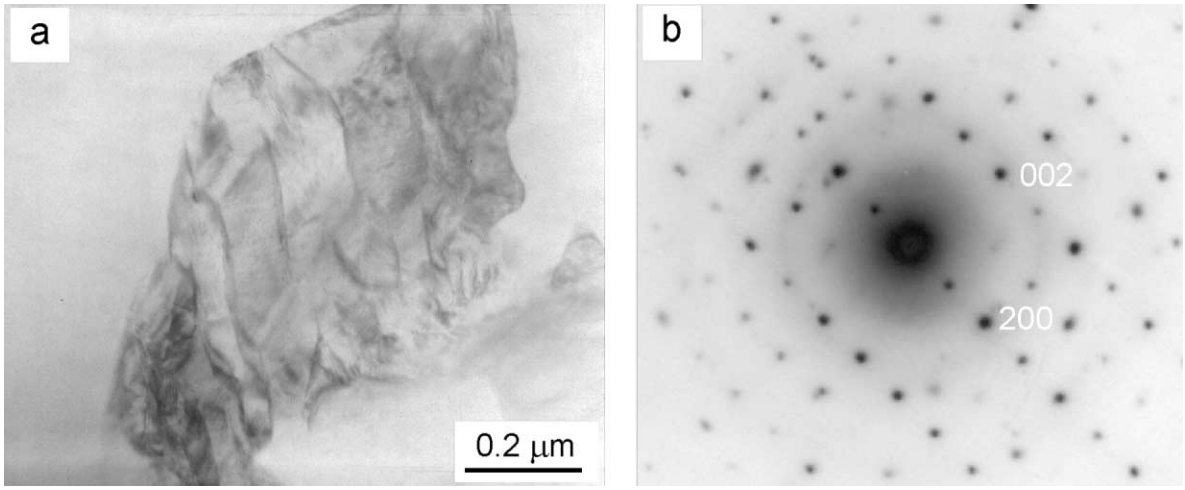

Fig. 7. (a) Bright field electron micrograph of a monoclinic particle of ZrO_2 stabilized with 11 mol% MgO showing martensitic plates and (b) corresponding selected area diffraction patterns at zone axis $[0\bar{1}0]$ m-ZrO_2. Note the different spacing in $<100>$ and $<001>$ directions.

was also found in grain 1 (Fig. 4b) and at the grain boundary (Fig. 4d), after small tilting in comparison with Fig. 4c. The orientation of grain 2 was quite different (Fig. 4f). This observation suggests the same behaviour as for the discontinuous precipitation in metallic alloys where the crystallographic orientation of the zone swept by the moving reaction front followed that of the matrix solid solution from which the growth initiated.

A detailed point to point EDX analysis was performed within the eutectoid products. Fig. 5a shows the results of the line-scan across the moving reaction front. One can see is very sharp change in the MgO content between the cubic matrix and m-ZrO_2 cell. This confirms that the eutectoid reaction in ZrO_2–MgO ceramics is controlled by interface rather than volume diffusion. Simultaneously, as it is shown in the Fig. 5b, the m-ZrO_2 cell is not uniformly MgO-depleted. The concentration profile shows a typical reverse "U" shape character, which was asymmetrical due to the previously mentioned pinning effect and the formation of subsequent MgO-rods at the moving interface.

Fig. 6 presents another area after eutectoid decomposition, where the formation of monoclinic ZrO_2 and MgO precipitates of rectangular or rod morphology was observed. The upper area in Fig. 6 was transformed to the m-ZrO_2 phase (Fig. 6c) and reveals a plate-like morphology containing fine modulations (Fig. 6a). Such modulations were previously observed by Farmer et al.[3] in the m-ZrO_2 phase formed due to the martensitic transformation. Rectangular precipitates of MgO are also visible in this figure. The lower part of the same area (Fig. 6b) consists of the tetragonal phase (Fig. 6d) while the surrounding grains are cubic (Fig. 6b and e). The enlarged monoclinic particle in the tetragonal ZrO_2 is also shown in Fig. 7.

4. Conclusions

In the early stages of the decomposition in ZrO_2 doped with 8.0 and 11.0 mol% MgO two different morphologies of eutectoid decomposition were observed. The first one, consisted of MgO-depleted t-ZrO_2 and MgO-rich phases of irregular shape growing in the grain interior. MgO-rich precipitates revealed either partially amorphous or monocrystalline structure. The second morphology was formed after prior grain boundary movement and it consisted of alternate phases: MgO-rich rods and MgO-depleted m-ZrO_2.

Application of energy dispersive X-ray spectroscopy led to the detection of the abrupt change in MgO content in the m-ZrO_2 phase, indicating that the eutectoid decomposition in ZrO_2–MgO is controlled by interface rather than volume diffusion. Simultaneously, eutectoid products of the "cellular" type preserve the same crystallographic orientation like the grain from which the growth was initiated.

References

1. Hannik, R. H. J., Microstructural development of sub-eutectoid aged MgO-ZrO_2 alloys. *J. Mater Sci.*, 1983, **18**, 457–469.
2. Farmer, S. C., Heuer, A. H. and Hannik, R. H. J., Eutectoid decomposition of MgO-partially-stabilized ZrO_2. *J. Am. Ceram. Soc.*, 1987, **70**, 431–440.
3. Farmer, S. C., Mitchell T. E. and Heuer, A. H., Diffusional decomposition of c-ZrO_2 in Mg-PSZ. In *Advances in Ceramics, Vol. 12. Structure and Technology of Zirconia*, ed. N. Claussen, M. Rühle and A. H. Heuer. The American Ceramic Society, 1984, pp.152–163.
4. Zięba, P. and Gust, W., Analytical electron microscopy of discontinuous solid state reactions. *Internat. Mater. Rev.*, 1998, **43**, 70–97.
5. Fournelle, R. A. and Clarke, J. B., The genesis of cellular precipitation reaction. *Metall. Trans. A*, 1972, **3**, 2757–2767.